Self-consistent mean-field theory of asymmetric first-order structural phase transitions

W. C. Kerr
Olin Physical Laboratory, Wake Forest University, Winston-Salem, North Carolina 27109-7507 *
and Theoretical Division, Los Alamos National Laboratory, Los Alamos, New Mexico 87545

E. N. Butler
Olin Physical Laboratory, Wake Forest University, Winston-Salem, North Carolina 27109-7507
(Received 8 December 1995; revised manuscript received 20 February 1996)

The paper presents a self-consistent mean-field theory for a lattice-dynamical model that exhibits a first-order structural phase transition. In this model the phase transition is produced because the high-energy structure has lower vibrational frequencies than those of the low-energy structure. This mechanism produces higher entropy in the higher-energy structure and thereby drives a phase transition. These structure-dependent frequencies are produced by anharmonicity in the interparticle interaction. The approximate theory of the transition given here reduces the exact coupled equations of motion to a single mean-field equation by replacing coupling terms between neighbors with appropriate averages. This step produces an effective potential that is used to calculate self-consistently the averages that appear in it. Thermodynamic properties calculated by this method show that the system has a first-order phase transition for sufficiently large strength of the interparticle anharmonicity. Further properties of the system obtained by this method include a discontinuous change in the shape of the average displacement and free-energy vs temperature relations as a function of the anharmonicity strength. This feature may be related to the hysteresis seen in previously performed computer simulations on the model. The effective potential also determines the displacement probability distribution function. For the parameter values studied here this distribution has a single maximum with only small asymmetry about this maximum. [S0163-1829(96)07729-6]

I. INTRODUCTION

The microscopic mechanisms responsible for macroscopic features observed at first-order structural phase transitions continue to warrant and receive further attention. This paper is the third in a series[1,2] in which a specific mechanism for causing these transitions has been put forward and its consequences examined. The introductory sections of papers I and II survey the relevant history of the field and the motivations of our specific model. We refer the reader to those papers and do not repeat that material here. In this Introduction we will summarize the salient points and concentrate on the new work presented in this paper.

The essential features of our lattice-dynamical model are that (i) each particle moves in an asymmetrical double-well potential and (ii) the interparticle interactions are anharmonic. Consequently, nonlinear forces acting on each particle arise from both the on-site potential and the interactions with neighboring particles. The phase transition which occurs in this model does *not* have symmetry-breaking character; there is no symmetry to break due to the asymmetry of the on-site potential. Rather, we have characterized the transition as being *entropy driven*. The idea we want to convey derives from an explanation by Zener[3] of transitions in β-phase alloys which showed the importance of the vibrational contribution to the entropy. The asymmetry of the on-site potential provides an ordering tendency in the system, since the lower well of this potential is always energetically preferred. A competing tendency arises from the anharmonicity of the interparticle forces. These forces are structure dependent in a way that causes lower vibrational frequencies in the structure with higher energy, thereby increasing the entropy associated with that structure. Thus for sufficiently strong anharmonicity, when the temperature is increased to a critical temperature, the structure with the higher internal energy achieves the lower free energy and a discontinuous change to that structure occurs.

Paper I presented extensive molecular dynamics (MD) calculations based on this model, but only a small portion of the parameter space could be covered by those calculations. Paper II presented an approximate theory, with the intention to survey qualitative features of the model over more of the parameter space. The theory presented in the second paper was a mean-field theory (MFT) with the additional assumption that the probability distribution function (PDF) for displacements is a Gaussian function. The justification for that additional assumption was an appeal to the simulations, which, over their limited parameter range, gave single-peaked, nearly symmetrical distributions. Since the purpose of paper II was to explain features seen in those simulations, this reasoning was somewhat circular. Nevertheless, by making that one additional assumption, the theory in paper II was able to elucidate other features seen in the simulations.

The present paper gives an improved approximate theory for the statistical mechanics of this model. This theory is a generalization of a theory for second-order structural phase transitions described in a review article by Bruce.[4] It is also a mean-field theory but without additional assumptions. As a result of this extended generality, we can calculate the displacement PDF rather than make an assumption about its shape. Thus this method can either justify or show the limitations of the assumption made in paper II. The ability to

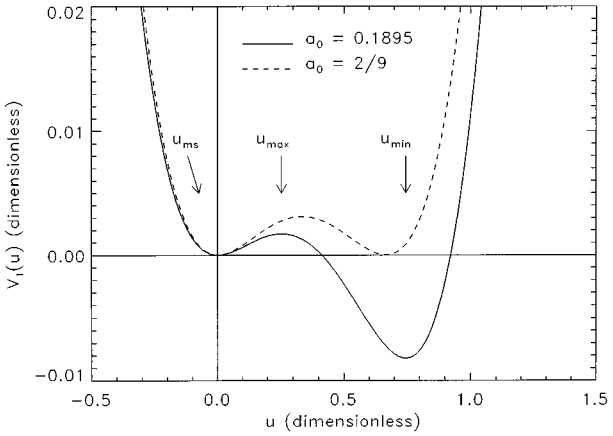

FIG. 1. The on-site potential [Eq. (2.2)] for the symmetric case $a_0 = 2/9$ and the asymmetric case for the value $a_0 = 0.1895$ used in the calculations. The arrows mark the metastable minimum, the maximum, and the stable minimum for the asymmetric case [Eq. (2.3)].

calculate this PDF is useful because one of the features of structural phase transitions that we are able to analyze with this model is the possibility of precursors of the transformation. These would be regions of the ''wrong'' phase appearing within a background of the phase corresponding to the existing temperature value. Such precursors would appear as multiple maxima in the displacement PDF. It is obviously impossible to find such features with a Gaussian assumption about the PDF.

In order to achieve the increased generality of this MFT, we must do self-consistent (SC) calculations of quantities appearing in the equation of motion for the system. For that reason we refer to this theory as the self-consistent mean-field theory (SCMFT).

We give a brief description of the model in Sec. II, derive the SCMFT equations in Sec. III, present some special cases of solutions in Sec. IV, and give low- and high-temperature asymptotic solutions in Sec. V before presenting solutions for the general case in Sec. VI. We give our conclusions in Sec. VII and discuss some numerical issues in the Appendix.

II. MODEL

The lattice-dynamical model exhibiting the phase transition is the same as was used for the computer simulations in paper I and the approximate theory in paper II. It is defined by the Hamiltonian

$$H=\sum_{\mathbf{n}} \frac{1}{2}p_{\mathbf{n}}^2+\sum_{\mathbf{n}} V_1(u_{\mathbf{n}})+\frac{1}{2}\sum_{\mathbf{n},\boldsymbol{\delta}} V_2(u_{\mathbf{n}},u_{\mathbf{n}+\boldsymbol{\delta}}). \quad (2.1)$$

Here $\mathbf{n}$ denotes the sites of a D-dimensional hypercubic lattice, $\boldsymbol{\delta}$ denotes the set of nearest-neighbor lattice vectors, and $u_{\mathbf{n}}$ is a scalar displacement variable at the $\mathbf{n}$th lattice site. The on-site potential energy $V_1(u)$ is (see Fig. 1)

$$V_1(u)=\frac{1}{2}a_0u^2-\frac{1}{3}u^3+\frac{1}{4}u^4. \quad (2.2)$$

[All quantities in this paper are scaled to dimensionless values, using the factors given in Table II of paper I. For example, the particle mass in Eq. (2.1) is $M = 1$.] For $a_0=2/9$, $V_1(u)$ is a symmetric double-well potential with degenerate minima at $u=0$ and $u=2/3$ and a maximum at $u=1/3$. For this case and for *harmonic* interparticle interactions (see below), the system is known to have a *second-order* transition.[4] For $0<a_0<2/9$, it has a metastable minimum at $u_{\rm ms}$, a maximum at $u_{\rm max}$, and a stable minimum at $u_{\rm min}$, which are given by

$$u_{\rm ms}=0, \quad u_{\rm max}=\frac{1}{2}[1-\sqrt{1-4a_0}]<\frac{1}{3},$$

$$u_{\rm min}=\frac{1}{2}[1+\sqrt{1-4a_0}]>\frac{2}{3}. \quad (2.3)$$

The pair interaction energy is

$$V_2(u,u')=\frac{1}{2}[k+\alpha(u+u')](u-u')^2, \quad (2.4)$$

where k is the interparticle harmonic force constant. The parameter α is referred to as the anharmonicity parameter throughout the paper; our major concern is to see how the system properties change with increasing anharmonicity strength. The motivation for choosing this model potential energy function is given in detail in papers I and II to which the reader is referred. The essential idea is to stabilize the higher-energy structure at higher temperatures by having higher vibrational entropy.[3] The function $V_2(u,u')$ achieves this effect by decreasing the effective force ''constant'' of the interparticle interaction when the particles are near the metastable minimum of the on-site potential. The weaker forces produce lower vibrational frequencies, which leads to increased entropy.

The phase transition occurring in this model for $a_0<2/9$ and $\alpha\neq 0$ is non-symmetry-breaking, because of the asymmetry of the on-site potential. Another model based on the same physical idea but for symmetry-breaking transitions has been studied by Gooding and Morris.[5] That model utilizes the ϕ^6 potential and a symmetric interparticle interaction.

The exact equations of motion obtained from the Hamiltonian in Eqs. (2.1), (2.2), and (2.4) are

$$\frac{d^2u_{\mathbf{n}}}{dt^2}=-(a_0+2Dk)u_{\mathbf{n}}+(1-3D\alpha)u_{\mathbf{n}}^2-u_{\mathbf{n}}^3+k\sum_{\boldsymbol{\delta}} u_{\mathbf{n}+\boldsymbol{\delta}}$$

$$+\frac{1}{2}\alpha\sum_{\boldsymbol{\delta}} u_{\mathbf{n}+\boldsymbol{\delta}}^2+\alpha u_{\mathbf{n}}\sum_{\boldsymbol{\delta}} u_{\mathbf{n}+\boldsymbol{\delta}}. \quad (2.5)$$

We used the fact that the coordination number of a D-dimensional hypercubic lattice is $2D$ to write this equation, and we separated terms which involve only the $\mathbf{n}$th particle from terms which also involve its neighbors.

The parameter values used here for a_0, D, and k are the same as those used for the simulations in paper I; their determination is described in detail there. The values were chosen so that the model would represent the phase transition in Zr between the bcc phase and the ω phase. The structural distortion which occurs at this transformation is related to a particular low-lying phonon mode, making this transition a candidate for the mechanism considered in this paper. Because the focus of our enquiry into the model is to find how

the properties of the system change with the strength of the interparticle anharmonicity, we present results for many different α values. The value used for the interparticle harmonic force constant k is rather large, corresponding to the so-called displacive regime where site-dependent variables change slowly with **n** and a continuum approximation would be valid for the equation of motion.

III. SELF-CONSISTENT MEAN-FIELD THEORY

Mean-field theory (MFT) assumes that the particles move independently, so that the phase space PDF factors into single-particle functions,[6] i.e.,

$$F_N(\{p_{\mathbf{n}},u_{\mathbf{n}}\})=\prod_{\mathbf{n}} F_1(p_{\mathbf{n}},u_{\mathbf{n}})=\prod_{\mathbf{n}} \frac{e^{-p_{\mathbf{n}}^2/2T}}{\sqrt{2\pi T}}P_1(u_{\mathbf{n}}). \tag{3.1}$$

In the last step we introduced the Maxwell-Boltzmann distribution for the momenta at temperature T (Boltzmann's constant is unity in our dimensionless units); $P_1(u)$ is the single-particle displacement PDF. Because of this factorization of F_N, the conditional PDF for all other particles, given prescribed values for the variables of the **n**th particle, is obtained by omitting the factor for the **n**th particle from the product. We average Eq. (2.5), the exact equation of motion, over this conditional distribution to obtain the MFT equation of motion. The resulting single-particle equation is the same for all particles, and so we replace $u_{\mathbf{n}}$ by a generic displacement variable u; the result is

$$\frac{d^2u}{dt^2}=-[a_0+2Dk-2D\alpha\langle u\rangle]u+(1-3D\alpha)u^2-u^3 +2Dk\langle u\rangle+D\alpha\langle u^2\rangle. \tag{3.2}$$

The force on the right-hand side of Eq. (3.2) is derivable from a potential, and so we write

$$\frac{d^2u}{dt^2}=-\frac{\partial V_{\rm eff}}{\partial u}; \tag{3.3}$$

the temperature-dependent effective potential is

$$V_{\rm eff}(u;\langle u\rangle,\langle u^2\rangle)=C(T)-[2Dk\langle u\rangle+D\alpha\langle u^2\rangle]u +\frac{1}{2}[a_0+2Dk-2D\alpha\langle u\rangle]u^2 -\frac{1}{3}(1-3D\alpha)u^3+\frac{1}{4}u^4, \tag{3.4}$$

where $C(T)$ is a temperature-dependent integration constant.

Averages are computed from the effective potential according to the usual Gibbs distribution

$$\langle A\rangle=\frac{1}{Z_c(T)}\int_{-\infty}^{\infty}duA(u)\exp\left(-\frac{V_{\rm eff}(u;\langle u\rangle,\langle u^2\rangle)}{T}\right), \tag{3.5}$$

where

$$Z_c(T)=\int_{-\infty}^{\infty}du\exp\left(-\frac{V_{\rm eff}(u;\langle u\rangle,\langle u^2\rangle)}{T}\right) \tag{3.6}$$

is the single-particle configurational partition function. In particular, when this distribution is applied to calculate the averages which appear in $V_{\rm eff}$, we obtain the *self-consistent mean-field-theory* (SCMFT) equations:

$$\langle u\rangle=\frac{1}{Z_c(T)}\int_{-\infty}^{\infty}duu\exp\left(-\frac{V_{\rm eff}(u;\langle u\rangle,\langle u^2\rangle)}{T}\right), \tag{3.7}$$

$$\langle u^2\rangle=\frac{1}{Z_c(T)}\int_{-\infty}^{\infty}duu^2\exp\left(-\frac{V_{\rm eff}(u;\langle u\rangle,\langle u^2\rangle)}{T}\right). \tag{3.8}$$

These are a set of equations to be *solved* for $\langle u\rangle$ and $\langle u^2\rangle$ rather than merely evaluated.

The integration constant $C(T)$ of Eq. (3.4) factors out of the integrals in Eqs. (3.5) and (3.6) and therefore cancels from the ratio in Eq. (3.5); it is not necessary to know this quantity to compute the averages. Accordingly we define a shifted effective potential

$$V_{\rm eff}^{(0)}(u;\langle u\rangle,\langle u^2\rangle)=V_{\rm eff}(u;\langle u\rangle,\langle u^2\rangle)-C(T). \tag{3.9}$$

Corresponding to this shift, we define $Z_c^{(0)}(T)$ by using $V_{\rm eff}^{(0)}$ in Eq. (3.6). The averages $\langle u\rangle$ and $\langle u^2\rangle$ can be calculated using the SCMFT equations with $V_{\rm eff}^{(0)}$ and $Z_c^{(0)}$.

From Eq. (3.5) we identify the displacement probability density function of Eq. (3.1) as

$$P_1(u)=\frac{1}{Z_c(T)}\exp\left(-\frac{V_{\rm eff}(u;\langle u\rangle,\langle u^2\rangle)}{T}\right) \tag{3.10}$$

(or the same equation using $V_{\rm eff}^{(0)}$ and $Z_c^{(0)}$). Once the solutions for $\langle u\rangle$ and $\langle u^2\rangle$ are obtained from the SCMFT equations for given values of the parameters a_0, D, k, α, and T, this probability density is determined. This capability to calculate $P_1(u)$ is one of the major improvements of this self-consistent theory over the method presented in paper II, which assumed that $P_1(u)$ is Gaussian. Specifically, we note that if $V_{\rm eff}$ comes out to be a double-well potential for some particular parameter values or temperature, then there are two maxima in $P_1(u)$.

We will show that the SCMFT equations typically have multiple solutions for a given T. To discriminate among these solutions, we introduce the free energy function (per particle value)

$$f=-\frac{1}{2}T\ln(2\pi T)-T\ln Z_c(T) \tag{3.11}$$

$$=-\frac{1}{2}T\ln(2\pi T)-T\ln Z_c^{(0)}(T)+C(T); \tag{3.12}$$

the first term is the kinetic energy contribution. The physical solution of the SCMFT equations is the one with the minimum free energy. This function *does* depend on the integration constant $C(T)$ in Eq. (3.4). Thus $C(T)$ must be determined if we are to use Eq. (3.11) or (3.12) to determine the equilibrium phase at each T and the transition temperature T_c. To determine $C(T)$ we use an alternative formula for the free energy per particle,

$$f=e-Ts, \tag{3.13}$$

in terms of the internal energy e and entropy s. The internal energy is obtained from the average value of the Hamiltonian in Eq. (2.1), $e=\langle H\rangle/N$, and the entropy from the distribution function in Eq. (3.1), $s=-\langle \ln F_N\rangle/N$. These averages can be obtained using Eq. (3.5) calculated with $V_{\rm eff}^{(0)}$ and $Z_c^{(0)}$ so that $C(T)$ does not appear. By requiring that the two ways to calculate f be equivalent, we obtain the integration constant $C(T)$.

The average kinetic energy is

$$\sum_{\mathbf{n}} \langle \tfrac{1}{2}p_{\mathbf{n}}^2\rangle = \tfrac{1}{2}NT, \tag{3.14}$$

and the average on-site potential energy is

$$\sum_{\mathbf{n}} \langle V_1(u_{\mathbf{n}})\rangle = N\left(\frac{1}{2}a_0\langle u^2\rangle - \frac{1}{3}\langle u^3\rangle + \frac{1}{4}\langle u^4\rangle\right). \tag{3.15}$$

To compute the average of the pair interaction terms, we first separate each pair interaction into single-particle and ''irreducible'' pair terms

$$\begin{aligned}\langle V_2(u_{\mathbf{n}},u_{\mathbf{n}+\boldsymbol{\delta}})\rangle &= \frac{1}{2}k[\langle u_{\mathbf{n}}^2\rangle + \langle u_{\mathbf{n}+\boldsymbol{\delta}}^2\rangle - 2\langle u_{\mathbf{n}}u_{\mathbf{n}+\boldsymbol{\delta}}\rangle] \\ &\quad + \frac{1}{2}\alpha[\langle u_{\mathbf{n}}^3\rangle + \langle u_{\mathbf{n}+\boldsymbol{\delta}}^3\rangle - \langle u_{\mathbf{n}}^2u_{\mathbf{n}+\boldsymbol{\delta}}\rangle \\ &\quad - \langle u_{\mathbf{n}}u_{\mathbf{n}+\boldsymbol{\delta}}^2\rangle].\end{aligned} \tag{3.16}$$

Since we assumed factorization of the distribution in Eq. (3.1), the averages of products involving different particles in Eq. (3.16) factor into products of averages. Then the average pair interaction energy is

$$\begin{aligned}\frac{1}{2}\sum_{\mathbf{n},\boldsymbol{\delta}} \langle V_2(u_{\mathbf{n}},u_{\mathbf{n}+\boldsymbol{\delta}})\rangle &= \frac{1}{2}N(2D)\{k[\langle u^2\rangle - \langle u\rangle^2] \\ &\quad + \alpha[\langle u^3\rangle - \langle u^2\rangle\langle u\rangle]\}.\end{aligned} \tag{3.17}$$

The internal energy of the system is the sum of Eqs. (3.14), (3.15), and (3.17).

To compute the entropy we need, from Eqs. (3.1) and (3.10),

$$\begin{aligned}\langle \ln F_1\rangle &= -\frac{1}{T}\langle \tfrac{1}{2}p^2\rangle - \tfrac{1}{2}\ln(2\pi T) - \frac{1}{T}\langle V_{\rm eff}^{(0)}(u;\langle u\rangle,\langle u^2\rangle)\rangle \\ &\quad - \ln Z_c^{(0)}(T),\end{aligned} \tag{3.18}$$

and from Eqs. (3.4) and (3.9),

$$\begin{aligned}\langle V_{\rm eff}^{(0)}(u;\langle u\rangle,\langle u^2\rangle)\rangle &= -[2Dk\langle u\rangle + D\alpha\langle u^2\rangle]\langle u\rangle \\ &\quad + \frac{1}{2}[a_0 + 2Dk - 2D\alpha\langle u\rangle]\langle u^2\rangle \\ &\quad - \frac{1}{3}(1-3D\alpha)\langle u^3\rangle + \frac{1}{4}\langle u^4\rangle.\end{aligned} \tag{3.19}$$

Using the result for the average kinetic energy in Eq. (3.14), the entropy per particle s is

$$\begin{aligned}s &= +\frac{1}{2} + \frac{1}{2}\ln(2\pi T) + \frac{1}{2}[a_0 + 2Dk - 2D\alpha\langle u\rangle]\frac{\langle u^2\rangle}{T} \\ &\quad + \ln Z_c^{(0)}(T) - \frac{1}{3}(1-3D\alpha)\frac{\langle u^3\rangle}{T} + \frac{1}{4}\frac{\langle u^4\rangle}{T} \\ &\quad - [2Dk\langle u\rangle + D\alpha\langle u^2\rangle]\frac{\langle u\rangle}{T}.\end{aligned} \tag{3.20}$$

Combining Eqs. (3.14), (3.15), and (3.17) for the internal energy e and (3.20) for the entropy s, we obtain for the free energy per particle,

$$f = -\frac{1}{2}T\ln(2\pi T) - T\ln Z_c^{(0)}(T) + Dk\langle u\rangle^2 + D\alpha\langle u^2\rangle\langle u\rangle. \tag{3.21}$$

Comparing the two formulas for the free energy in Eqs. (3.12) and (3.21), we see that the integration constant in Eq. (3.4) is

$$C(T) = Dk\langle u\rangle^2 + D\alpha\langle u^2\rangle\langle u\rangle. \tag{3.22}$$

The single-particle effective potential is obtained by combining Eqs. (3.4) and (3.22). This function can be written in different ways that illustrate different aspects of its behavior. One way is, using Eq. (2.2),

$$\begin{aligned}V_{\rm eff}(u;\langle u\rangle,\langle u^2\rangle) &= V_1(u) + Dk(u-\langle u\rangle)^2 \\ &\quad + D\alpha(u-\langle u\rangle)(u^2-\langle u^2\rangle).\end{aligned} \tag{3.23}$$

This form emphasizes that the difference between the microscopic on-site potential and the effective potential is due to the interparticle interactions and is determined by the fluctuations in both u and u^2. By some manipulations $V_{\rm eff}$ can also be written in terms of both the microscopic on-site and interparticle potentials, as

$$\begin{aligned}V_{\rm eff}(u;\langle u\rangle,\langle u^2\rangle) &= V_1(u) + (2D)V_2(u,\langle u\rangle) \\ &\quad - (2D)\frac{1}{2}\alpha(u-\langle u\rangle)[\langle u^2\rangle - \langle u\rangle^2].\end{aligned} \tag{3.24}$$

This equation has been written to emphasize that the coordination number of the lattice is $2D$. One might have written the first two terms intuitively from Eq. (2.1) by asking for the potential energy that one particle experiences assuming that its neighbors are all displaced by $\langle u\rangle$. This last equation shows that such a procedure would omit the contribution arising from the fluctuations in u^2.

An alternate method to calculate these properties is the self-consistent phonon theory (SCPT). This method takes the Fourier amplitudes of the displacement field as the fundamental variables. Its central assumptions are that the phase space PDF factors into a product of individual mode PDF's and that the factor for each Fourier mode is Gaussian. This assumption is exact for a purely harmonic Hamiltonian; for anharmonic systems the SCPT gives the best (in a variational sense) harmonic approximation. For the case of no anharmonicity ($\alpha = 0$) and a symmetric on-site potential ($a_0 = 2/9$), it is known[7] that the SCPT predicts a first-order transition, in contradiction to the known occurrence of a second-order transition. Thus for this limiting case, our MFT gives the more accurate description (see Sec. IV). The product of Gaussian factors for the Fourier amplitudes transforms to a multivariate Gaussian in terms of the displacements, i.e., a function of the form $\exp(-\Sigma_{ij} u_i A_{ij} u_j)$. When this is integrated over all but one of the displacements to obtain the single particle PDF, the result is again a Gaussian. This is the same form that was assumed for the displacement PDF in paper II. However, the parameters in these Gaussians are determined by different prescriptions, and so it is impossible to compare further the results of the two theories without doing the SCPT calculations.

IV. ZERO INTERPARTICLE ANHARMONICITY

We first describe the solutions of the SCMFT equations [Eqs. (3.7) and (3.8)] for the special case of no interparticle anharmonicity, in order to set the stage for the more complicated $\alpha \neq 0$ case to follow. When $\alpha = 0$, the effective potential simplifies to

$$V_{\text{eff}}(u;\langle u\rangle,\langle u^2\rangle) = V_1(u) + Dk(u-\langle u\rangle)^2. \tag{4.1}$$

This function no longer contains $\langle u^2\rangle$, and so in this limit there is only one SCMFT equation to be solved, viz., Eq. (3.7).

There are two cases of interest here: the symmetric on-site potential for $a_0 = 2/9$ and the asymmetric case $a_0 < 2/9$. We discuss each in turn.

A. $a_0 = 2/9$

With $a_0 = 2/9$ the on-site potential can be written

$$V_1(u) = \frac{1}{4}u^2\left(u - \frac{2}{3}\right)^2. \tag{4.2}$$

This is a double well with degenerate minima at $u = 0$ and $u = 2/3$; it is symmetric about the maximum at $u = 1/3$ (see Fig. 1). If the origin is shifted to $u = 1/3$, then one sees that this model is a lattice version of the much-studied ϕ^4 field theory. It is known[4] to have a second-order phase transition for $D \geq 2$.

In Eq. (3.7), evaluated for the parameter values of this section, we change the integration variable by $u = 1/3 + x$, $\langle u\rangle = 1/3 + \langle x\rangle$; the result is

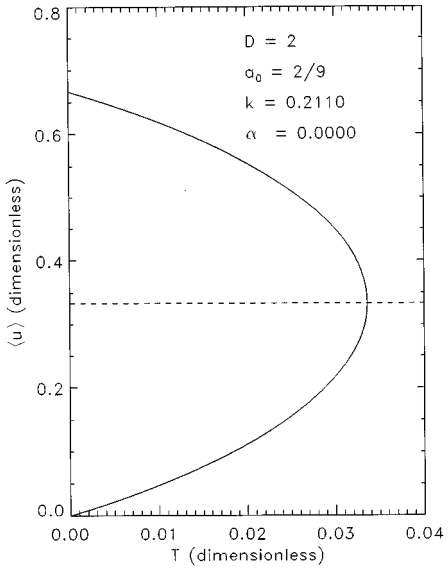

FIG. 2. Average displacement vs temperature for the symmetric on-site potential and zero interparticle anharmonicity. The solid curve is the stable broken-symmetry solution below T_c. The dashed line is the unstable solution below T_c and the only solution above T_c [Eq. (4.4)].

$$\langle x\rangle = \frac{\int_{-\infty}^{\infty} dx\, x \exp\left[-\left(x^2 - \frac{1}{9}\right)^2 \Big/ 4T - Dk(x-\langle x\rangle)^2/T\right]}{\int_{-\infty}^{\infty} dx \exp\left[-\left(x^2 - \frac{1}{9}\right)^2 \Big/ 4T - Dk(x-\langle x\rangle)^2/T\right]}. \tag{4.3}$$

On the right-hand side of Eq. (4.3), we put $\langle x\rangle = 0$; the resulting numerator integral vanishes because of the odd parity of the integrand. So $\langle x\rangle = 0$ or

$$\langle u\rangle = \frac{1}{3}, \quad 0 \leq T < \infty, \tag{4.4}$$

is one solution of the SCMFT equation for all temperatures, for these parameter values.

Now suppose that some other value $\langle x\rangle > 0$ is a solution of Eq. (4.3). On the right-hand side, we substitute the value $-\langle x\rangle < 0$ into the integrals and then change the integration variables to $x' = -x$. The resulting ratio of integrals is equal to $-\langle x\rangle$, proving that $-\langle x\rangle$ solves Eq. (4.3) if $\langle x\rangle$ does. In terms of $\langle u\rangle$, solutions other than Eq. (4.4) appear in pairs, symmetrically located about the line $\langle u\rangle = 1/3$.

Figure 2 shows the numerical solution of Eq. (3.7) for a particular set of parameters. The solid curves are solutions symmetrically located about the line $\langle u\rangle = 1/3$, as described above. They show $\langle u\rangle$ developing out of either of the degenerate minima of the on-site potential as T is increased. The dashed line is the other solution, which satisfies the SCMFT equation for all temperatures, Eq. (4.4). As expected we get a second-order, symmetry-breaking transition with $T_c \approx 0.0337$. The MFT in paper II, based on the assumption of a Gaussian distribution for $P_1(u)$, gave $T_c \approx 0.031$. Figure 3 shows the free energy for this case, evaluated from Eq. (3.21). The solid line is the equilibrium free energy for $T < T_c$, since it is the minimum value over that temperature

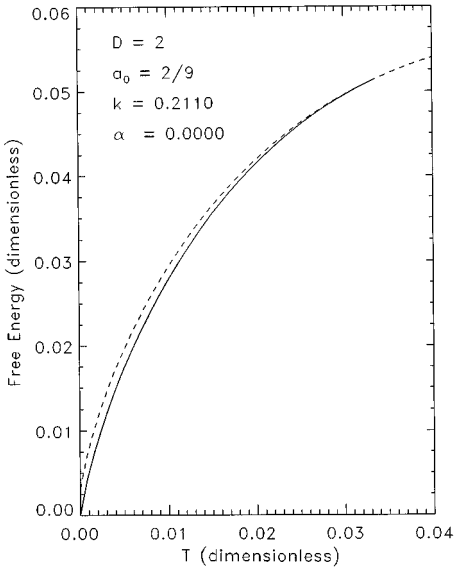

FIG. 3. Free energy vs temperature for the solution shown in Fig. 2. The solid curve is the free energy for both the top and bottom halves of the solid curve in Fig. 2, and the dashed curve is the free energy for the dashed line in Fig. 2.

interval. It is the free energy for both the top and bottom parts of the solid curve for $\langle u \rangle$ vs T in Fig. 2. The dashed curve in Fig. 3 corresponds to the other solution for $\langle u \rangle$, Eq. (4.4). At T_c the two solutions join continuously with continuous first derivative (entropy) and discontinuous second-derivative (specific heat).

B. $a_0 < 2/9$

Figure 4 shows the numerical solution of Eq. (3.7) for the asymmetrical double well in the on-site potential, and Fig. 5

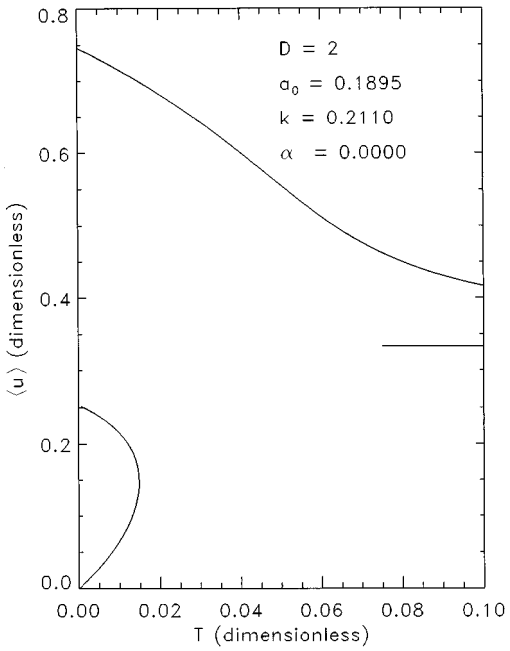

FIG. 4. Average displacement vs temperature for the asymmetric on-site potential and zero interparticle anharmonicity. The short horizontal line on the right is the line $\langle u \rangle = 1/3$, which is the horizontal asymptote of the solution [Eq. (5.34)].

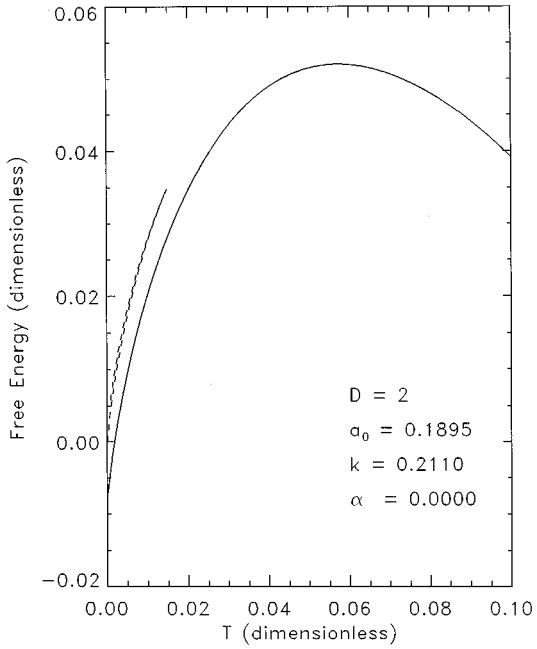

FIG. 5. Free energy vs temperature for the solution shown in Fig. 4. The solid curve corresponds to the top branch, and the dashed curve is a very narrow loop corresponding to the bottom branch. The two intercepts of the dashed curve with the $T = 0$ axis are the values $V_1(0)$ and $V_1(u_{\max})$ [Eq. (5.18)].

shows the branches of the free energy corresponding to the $\langle u \rangle$ vs T graph. The character of the solution is very different from the previous subsection.

The physical solution for $\langle u \rangle$ is the top branch in Fig. 4. It evolves out of the stable minimum of $V_1(u)$ and smoothly approaches an asymptote as T increases. There is no discontinuity or singularity in the $\langle u \rangle$ vs T graph. Making the on-site potential asymmetric destroys the phase transition that is present for the symmetric case. This result was seen earlier in papers I and II and is discussed in those papers.

There is another branch to the $\langle u \rangle$ vs T relation, which itself is double valued (the lower branch). It intercepts the $T = 0$ axis at both $\langle u \rangle = u_{\rm ms} = 0$ and $\langle u \rangle = u_{\max}$. The corresponding free energy values form a very narrow loop on the $f(T)$ graph (Fig. 5); at each T this solution lies above the one described in the previous paragraph, and so this branch is never the physical solution.

Some features of these $\langle u \rangle$ vs T and free energy graphs persist when the interparticle anharmonicity described by α is included. For example, on the $\langle u \rangle$ vs T graphs, there are intercepts at all of the extrema of the $V_1(u)$ function: $u_{\rm ms}$, $u_{\max}$, and $u_{\min}$. Additional foldings and unfoldings occur as α is included, and we now turn to an analysis of those features.

V. ASYMPTOTIC EXPANSIONS

We showed some examples of average displacement $\langle u \rangle$ vs T and free energy f vs T graphs for simple cases with no interparticle anharmonicity in Sec. IV. Section VI contains results for the case including the interparticle anharmonicity. The evolution of the properties with increasing α, obtained

from numerical solution of the SCMFT equations [Eqs. (3.7) and (3.8)], is somewhat intricate. To follow this evolution, it is helpful to have analytic asymptotic results for low- and high-temperature limits. The derivation of these results is outlined in this section.

The effective potential $V_{\rm eff}$ in Eq. (3.4) approaches $+\infty$ for $u\to\pm\infty$, and so it has an absolute minimum at some value of the displacement which we call $u_p(T)$. From Eq. (3.10), $u_p(T)$ is also the absolute maximum of the displacement probability density; i.e., it is the most likely displacement. It is the solution of the equation $V'_{\rm eff}(u_p(T);\langle u\rangle,\langle u^2\rangle)=0$ or

$$V_1'(u_p)+2Dk(u_p-\langle u\rangle)+D\alpha[3u_p^2-2u_p\langle u\rangle-\langle u^2\rangle]=0, \tag{5.1}$$

which has the property

$$V''_{\rm eff}(u_p;\langle u\rangle)\equiv V_1''(u_p)+2Dk+2D\alpha[3u_p-\langle u\rangle]>0. \tag{5.2}$$

Note that $V''_{\rm eff}(u_p;\langle u\rangle)$ does not depend on $\langle u^2\rangle$. Since Eq. (5.1) is cubic in $u_p(T)$, it may have either one or three real roots; in either case $u_p(T)$ denotes the location of the absolute minimum of $V_{\rm eff}$.

We now change variables by shifting the origin according to $u=u_p(T)+x$; the quartic polynomial $V_{\rm eff}$ is then exactly expressed as

$$\begin{aligned}V_{\rm eff}(u_p+x;\langle u\rangle,\langle u^2\rangle)=&V_{\rm eff}(u_p;\langle u\rangle,\langle u^2\rangle)\\&+\frac{1}{2}V''_{\rm eff}(u_p;\langle u\rangle)x^2\\&+[u_p(T)-u_3(\alpha)]x^3+\frac{1}{4}x^4;\end{aligned} \tag{5.3}$$

we introduced here a constant displacement defined by

$$u_3(\alpha)=\frac{1}{3}(1-3D\alpha), \tag{5.4}$$

which appears in the coefficient of the cubic term. Because $u_p(T)$ is an extremum of $V_{\rm eff}$, there is no linear term in Eq. (5.3). Since the displacement probability density $P_1(u)$ [Eq. (3.10)] is proportional to $\exp(-V_{\rm eff}/T)$, Eq. (5.3) shows that asymmetry of this distribution about its maximum is governed by the magnitude and sign of $[u_p(T)-u_3(\alpha)]$. Using Eq. (5.3), the SCMFT equations can then be written as ratios of ''moments,'' $\langle u\rangle=M_1/M_0$, $\langle u^2\rangle=M_2/M_0$, where

$$\begin{aligned}M_n=&e^{-V_{\rm eff}(u_p;\langle u\rangle,\langle u^2\rangle)/T}\int_{-\infty}^{\infty}dx(u_p+x)^n\\&\times e^{-[V''_{\rm eff}(u_p;\langle u\rangle)x^2/2+(u_p-u_3)x^3+x^4/4]/T}.\end{aligned} \tag{5.5}$$

We obtain both low- and high-temperature expansions of the SCMFT equations from Eq. (5.5).

A. Low-temperature expansion

For low temperature we scale the coefficient of the quadratic term in the exponent of Eq. (5.5) to unity by changing the integration variable to $y=[V''_{\rm eff}(u_p;\langle u\rangle)/2T]^{1/2}x$; Eq. (5.2) assures that the square root factor is real. After cancelling common factors, the SCMFT equations become

$$\langle u\rangle=\frac{m_1}{m_0},\quad \langle u^2\rangle=\frac{m_2}{m_0}, \tag{5.6}$$

where the low-temperature reduced moments are defined by

$$\begin{aligned}m_n=&\int_{-\infty}^{\infty}dye^{-y^2}\left(u_p+\sqrt{\frac{2T}{V''_{\rm eff}(u_p;\langle u\rangle)}}y\right)^n\\&\times\exp\left\{-\frac{2^{3/2}(u_p-u_3)}{[V''_{\rm eff}(u_p;\langle u\rangle)]^{3/2}}T^{1/2}y^3\right.\\&\left.-\frac{1}{[V''_{\rm eff}(u_p;\langle u\rangle)]^2}Ty^4\right\}.\end{aligned} \tag{5.7}$$

This variable change has moved all explicit factors of T into numerators. For low T we expand the last exponential factor in Eq. (5.7) and evaluate the resulting Gaussian integrals. The results are

$$\frac{m_0}{\sqrt{\pi}}=1+\frac{3}{4}\frac{1}{[V''_{\rm eff}(u_p;\langle u\rangle)]^2}\left\{-1+10\frac{(u_p-u_3)^2}{V''_{\rm eff}(u_p;\langle u\rangle)}\right\}T+\cdots, \tag{5.8}$$

$$\frac{m_1}{\sqrt{\pi}}=u_p+\left\{-\frac{3}{4}\frac{(5u_p-4u_3)}{[V''_{\rm eff}(u_p;\langle u\rangle)]^2}+\frac{15}{2}\frac{u_p(u_p-u_3)^2}{[V''_{\rm eff}(u_p;\langle u\rangle)]^3}\right\}T+\cdots, \tag{5.9}$$

and

$$\frac{m_2}{\sqrt{\pi}}=u_p^2+\left\{\frac{1}{V''_{\rm eff}(u_p;\langle u\rangle)}-\frac{3}{4}\frac{u_p(9u_p-8u_3)}{[V''_{\rm eff}(u_p;\langle u\rangle)]^2}+\frac{15}{2}\frac{u_p^2(u_p-u_3)^2}{[V''_{\rm eff}(u_p;\langle u\rangle)]^3}\right\}T+\cdots. \tag{5.10}$$

Even though these expansions appear to be in powers of T, they are actually more complicated because the variables $u_p(T)$ and $\langle u\rangle$ appearing in them are T dependent. However, we can use these equations in an iterative fashion. First, we note that the denominators remain nonzero at $T=0$, and so the values of the reduced moments at $T=0$ are just the first terms. We substitute these into Eq. (5.6) and get

$$\langle u\rangle_{T=0}=u_p(T=0),\quad \langle u^2\rangle_{T=0}=u_p^2(T=0). \tag{5.11}$$

With these results, Eq. (5.1) determining $u_p(T)$ reduces to

$$V_1'(u_p(T=0))=0. \tag{5.12}$$

This equation has three solutions which are the three extrema of the on-site potential [cf. Fig. 1 and Eq. (2.3)]:

$$u_p(T=0)=0,\quad u_{\rm max},\ \text{or}\ u_{\rm min}. \tag{5.13}$$

Then Eq. (5.11) gives three solutions for $\langle u\rangle$ at $T=0$,

$$\langle u\rangle_{T=0}=0,\quad u_{\rm max},\ \text{or}\ u_{\rm min}, \tag{5.14}$$

and correspondingly for $\langle u^2\rangle$,

$$\langle u^2\rangle = 0, \quad u_{\max}^2, \text{ or } u_{\min}^2. \tag{5.15}$$

In agreement with this result, Figs. 2 and 4 in Sec. IV for $\langle u\rangle$ vs T (and related figures in the next section) have three intercepts along the $T = 0$ axis. Note that these intercepts depend only on the on-site potential and are independent of α.

The *physical* solution is the one with the lowest free energy. It is intuitively clear that, of these three solutions, the stable one is $u_{\min}$. To obtain this result formally, we determine which solution gives the minimum result in Eq. (3.11). Since

$$Z_c(T) = \exp\left(-\frac{V_{\text{eff}}(u_p;\langle u\rangle,\langle u^2\rangle)}{T}\right)\sqrt{\frac{2T}{V''_{\text{eff}}(u_p;\langle u\rangle)}}m_0, \tag{5.16}$$

the low-temperature expansion of the free energy is, including the kinetic energy contribution and using Eq. (3.23),

$$\begin{aligned} f = {} & V_1(u_p) + Dk(u_p-\langle u\rangle)^2 + D\alpha(u_p-\langle u\rangle)(u_p^2-\langle u^2\rangle)^2 \\ & -\frac{1}{2}T\left[\ln(2\pi T)+\ln\left(\frac{2\pi T}{V''_{\text{eff}}(u_p;\langle u\rangle)}\right)\right] \\ & -\left\{-\frac{3}{4}\frac{1}{[V''_{\text{eff}}(u_p;\langle u\rangle)]^2}+\frac{15}{2}\frac{(u_p-u_3)^2}{[V''_{\text{eff}}(u_p,\langle u\rangle)]^3}\right\}T^2 \\ & +\cdots, \end{aligned} \tag{5.17}$$

where we used $\ln(1+x)\approx x$ for $|x|\ll 1$ to get the last term. At $T = 0$, all terms but the first term vanish, leaving

$$f(T=0) = V_1(u_p(T=0)). \tag{5.18}$$

This result confirms that the minimum free energy at $T = 0$ is obtained for the solution $u_p(T=0)=\langle u\rangle_{T=0}=u_{\min}$. These three $T=0$ solutions can be seen in Fig. (5).

Having obtained the $T = 0$ solutions, the first-order corrections in T for the moments m_n are obtained by evaluating the quantities in braces in Eqs. (5.8)–(5.10) at their $T = 0$ values. The results are

$$\frac{m_0}{\sqrt{\pi}} = 1+\frac{3}{4}\frac{1}{K_e^2}\left[-1+10\frac{1}{K_e}(u_e-u_3)^2\right]T+\cdots, \tag{5.19}$$

$$\frac{m_1}{\sqrt{\pi}} = u_p(T)+\left[-\frac{3}{4}\frac{1}{K_e^2}(5u_e-4u_3)+\frac{15}{2}\frac{1}{K_e^3}u_e(u_e-u_3)^2\right]T +\cdots, \tag{5.20}$$

and

$$\frac{m_2}{\sqrt{\pi}} = u_p^2(T)+\left[\frac{1}{K_e}-\frac{3}{4}\frac{1}{K_e^2}u_e(9u_e-8u_3) +\frac{15}{2}\frac{1}{K_e^3}u_e^2(u_e-u_3)^2\right]T+\cdots. \tag{5.21}$$

Since there are three $T = 0$ solutions, Eqs. (5.19)–(5.21) are actually three sets of equations, one set for each of the zero-temperature solutions. The subscript e denotes extremum; e.g., u_e denotes any of the three extrema of $V_1(u)$, $u_e=u_{\text{ms}}$, $u_{\max}$, or $u_{\min}$. In addition the constants K_e (one for each extremum) are defined as

$$K_e \equiv \lim_{T\to 0} V''_{\text{eff}}(u_p;\langle u\rangle) = V_1''(u_e)+2D(k+2\alpha u_e); \tag{5.22}$$

they are the effective zero-temperature force constants for moving one particle away from the extrema of V_1 (recall that $2D$ is the coordination number). The first terms on the right-hand sides of Eqs. (5.20) and (5.21) require the low-temperature values of $u_p(T)$. We write this as $u_p(T)=u_e+S_p^{(e)}T+\cdots$, where the coefficient $S_p^{(e)}$ is unknown, and we write similar expansions for $\langle u\rangle$ and $\langle u^2\rangle$. These low-temperature expansions can then be combined with Eq. (5.1) defining $u_p(T)$ and Eq. (5.6) to obtain the coefficients of the first-order temperature terms. The results are

$$u_p(T) = u_e-\frac{2D}{V_1''(u_e)K_e^2}\left[3(k+2\alpha u_e)(u_e-u_2) -\frac{1}{2}\alpha V_1''(u_e)\right]T+\cdots, \tag{5.23}$$

$$\langle u\rangle = u_e-\frac{3}{V_1''(u_e)K_e}(u_e-u_2)T+\cdots, \tag{5.24}$$

and

$$\langle u^2\rangle = u_e^2+\frac{1}{V_1''(u_e)K_e}[V_1''(u_e)-6u_e(u_e-u_2)]T+\cdots. \tag{5.25}$$

In Eq. (5.23)–(5.25) we introduced another constant displacement

$$u_2(\alpha) = \frac{1}{3}(1-2D\alpha). \tag{5.26}$$

Equations (5.23)–(5.25) are actually three sets of equations, corresponding to the three values of u_e. They describe how $u_p(T)$, $\langle u\rangle$, and $\langle u^2\rangle$ deviate from their $T = 0$ values. For example, the slope at each of the three $T = 0$ intercepts in Fig. 2 is given by Eq. (5.24). These results can be used in Eq. (5.17) to obtain a low-temperature expansion of the free energy.

The quantity K_e appearing in these low-T expansions suggests two different regions in parameter space. The quantity $V_1''(u_e=u_{\max})$ is negative, but has the positive quantity $2D(k+2\alpha u_{\max})$ added to it. The value of the harmonic force constant k used in the simulations in paper I and for the calculations here is sufficiently large that $V_1''(u_{\max})+2Dk$ is positive. This is one region of parameter space. The other region is for a smaller value of k such that $V_1''(u_{\max})+2D(k+2\alpha u_{\max})$ remains negative over the α range of interest. The slope of the $\langle u\rangle$ vs T graph at the $u_{\max}$ intercept would have the opposite sign, according to Eq. (5.24). This change in the shape of the $\langle u\rangle$ vs T graph suggests the possibility of different properties for weaker values of the harmonic force constant. We do not pursue this pos-

sibility in this paper, but instead continue with the parameter values used in the simulations in paper I.

B. High-temperature expansion

Expanding Eq. (5.5) directly in powers of $1/T$ gives divergent integrals, and so we need to find a convergence factor. First, we rewrite Eq. (5.5) so that the integration is over the interval $0<x<\infty$; then we change integration variables to $y=x^4/4T$ and obtain

$$M_n=\frac{1}{4}e^{-V_{\rm eff}(u_p;\langle u\rangle,\langle u^2\rangle)/T}(4T)^{1/4}\mu_n, \tag{5.27}$$

where the high-temperature reduced moments are

$$\mu_n=(4T)^{n/4}\int_0^\infty dy e^{-y}y^{1/4-1}\exp\left[-V''_{\rm eff}(u_p;\langle u\rangle)\frac{y^{1/2}}{T^{1/2}}\right]$$
$$\times\left(\left[\frac{u_p}{(4T)^{1/4}}-y^{1/4}\right]^n\exp\left[2^{3/2}(u_p-u_3)\frac{y^{3/4}}{T^{1/4}}\right]\right.$$
$$\left.+\left[\frac{u_p}{(4T)^{1/4}}+y^{1/4}\right]^n\exp\left[-2^{3/2}(u_p-u_3)\frac{y^{3/4}}{T^{1/4}}\right]\right). \tag{5.28}$$

This variable change has moved all explicit factors of T in the integrand into denominators. In terms of μ_n the SCMFT equations are the same as Eq. (5.6) with m_n replaced by μ_n. The e^{-y} factor in μ_n provides convergence when the other factors are expanded in $1/T$. As in the previous subsection, to obtain the correct asymptotic expansion in powers of $1/T$, the implicit dependence of $u_p(T)$ and $\langle u\rangle$ on T must be included.

The dominant $T\to\infty$ behavior of μ_n is obtained by expanding the exponentials in the previous equation for small arguments. To lowest order,

$$\mu_0=2\Gamma(1/4)+\cdots, \tag{5.29}$$

$$\mu_1=2\Gamma(1/4)u_3+2\Gamma(3/4)[V''_{\rm eff}(u_p;\langle u\rangle)(2u_p-3u_3)$$
$$+(u_p-u_3)^2(-4u_p+7u_3)]\frac{1}{T^{1/2}}+\cdots, \tag{5.30}$$

$$\mu_2=4\Gamma(3/4)T^{1/2}+\cdots, \tag{5.31}$$

where omitted terms are higher order in $1/T$ and $\Gamma(x)$ is the gamma function. The second part of Eq. (5.6) (but using the high-temperature moments) gives explicitly

$$\langle u^2\rangle=\frac{2\Gamma(3/4)}{\Gamma(1/4)}T^{1/2}+\cdots. \tag{5.32}$$

This unbounded behavior of $\langle u^2\rangle$ with increasing T is quite reasonable.

With this result, we return to Eq. (5.1) to obtain the high-temperature behavior of $u_p(T)$. We assume, subject to verification, that $\langle u\rangle$ approaches a constant as $T\to\infty$. Since the $D\alpha\langle u^2\rangle$ term grows without bound as $T\to\infty$, $u_p(T)$ must also become large, and so the $u_p^3(T)$ term in $V_1'(u_p)$ dominates. The highest-order term of $u_p(T)$, the most likely displacement, is then

$$\lim_{T\to\infty}u_p(T)=(D\alpha\langle u^2\rangle)^{1/3}=\left(\frac{2\Gamma(3/4)}{\Gamma(1/4)}D\alpha\right)^{1/3}T^{1/6}. \tag{5.33}$$

These results, together with the first of Eq. (5.6) (using the high-temperature moments), finally give

$$\lim_{T\to\infty}\langle u\rangle=u_\infty(\alpha)\equiv u_3(\alpha)+\left[\frac{2\Gamma(3/4)}{\Gamma(1/4)}\right]^2D\alpha$$
$$=\frac{1}{3}\left\{1-3\left(1-\left[\frac{2\Gamma(3/4)}{\Gamma(1/4)}\right]^2\right)D\alpha\right\}. \tag{5.34}$$

The coefficient of $D\alpha$ in this equation is negative, and so $u_\infty(\alpha)$ decreases with increasing α, and even becomes negative for sufficiently large α. The value $u_\infty(\alpha=0)=1/3$ was seen in Sec. IV as the high-temperature asymptote in Fig. 4. Note that this value depends only on the parameters D and α and is independent of a_0 and k.

Equation (5.32) for $\langle u^2\rangle$ is the same as the mean-square displacement of a single particle moving in a purely quartic potential $V_1(u)=u^4/4$. Therefore Eq. (5.32) shows that for $T\to\infty$ this particular property depends only on the high-energy part of the on-site potential; it becomes insensitive to other details, e.g., the shape of the double well (determined by a_0) and the strength of the interparticle interactions (determined by k and α). In contrast to this result for the second moment of the PDF, Eqs. (5.33) and (5.34) show that the limiting values of the *mean* value $\langle u\rangle$ and the *most likely* value $u_p(T)$ depend only on the strength of the interparticle anharmonicity α and are independent of the other parameters. In the high-temperature limit these different properties of the PDF are described by disjoint parameter sets. These equations also show that $\langle u\rangle$ approaches a constant (as assumed above), whereas $u_p(T)$ moves out to infinity, as $T\to\infty$. The situation of the most likely value and the average value being markedly different is unusual in statistical mechanics, where one often assumes that the average and most likely values are indistinguishable. Finally, we note that since the PDF is normalized at all T and since the separation between its peak and its mean diverges as $T\to\infty$, it becomes very flat in this limit. Equation (3.10) then shows that the same is true for the effective potential.

Continuing the expansion of the SCMFT equations to higher order in $1/T$ shows that the expansion parameter here is $1/T^{1/6}$. Thus, the approach to the asymptotic limits is quite slow.

VI. NONZERO INTERPARTICLE ANHARMONICITY

In this section we present the solutions of the SCMFT equations [Eqs. (3.7) and (3.8)] including interparticle anharmonicity, $\alpha\neq0$, which demonstrate that first-order phase transitions occur for sufficiently large values of α. First we show the results for the average displacement and free energy; then we show the results for the displacement PDF. The solutions for $\alpha=0$ in Sec. IV and the small- and large-T asymptotic results in Sec. V provide limiting cases for following how the properties change with increasing strength of the interparticle anharmonicity.

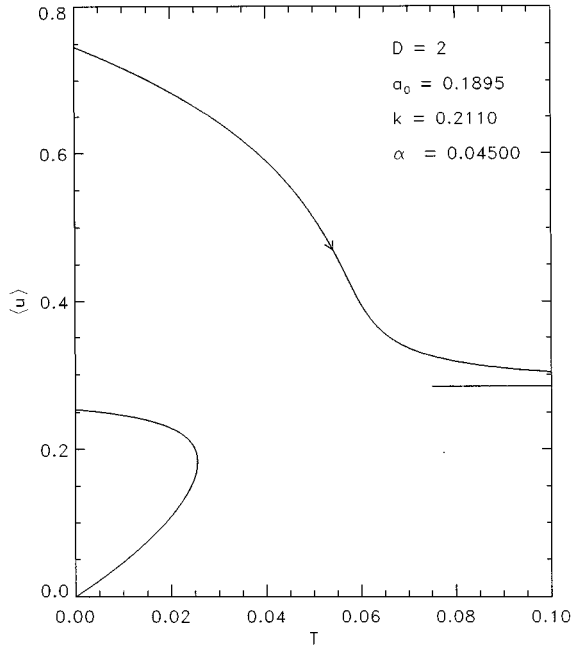

FIG. 6. Average displacement vs temperature for $\alpha = 0.045$. The three intercepts going up the $T = 0$ axis are at 0, $u_{\max}$, and $u_{\min}$ [Eq. (5.14)]. The short horizontal line at the right is the high temperature asymptote $u_\infty(\alpha)$ [Eq. (5.34)]. The arrow shows the equilibrium states followed by the system for increasing T.

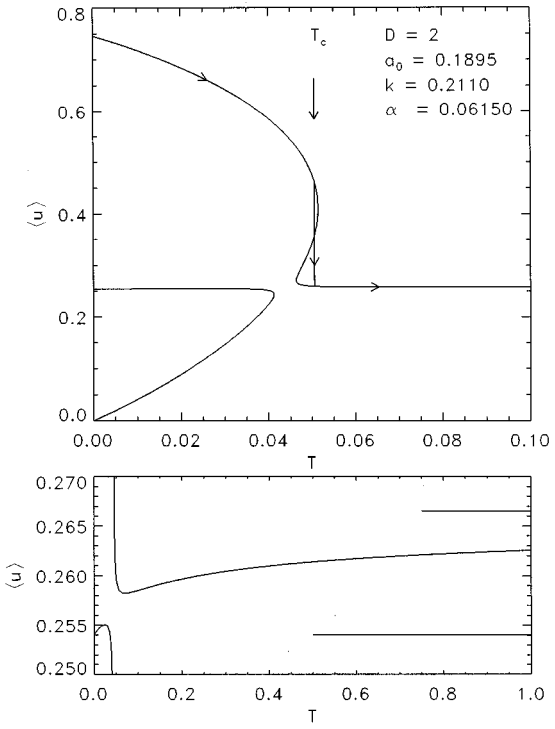

FIG. 7. Average displacement vs temperature for $\alpha = 0.0615$. The top panel shows the low-temperature range. The arrows on the curve show the equilibrium states followed by the system for increasing T. The vertical line cutting across the top branch shows the discontinuity in $\langle u \rangle$ at T_c. The bottom panel has a compressed temperature scale, and an expanded scale for $\langle u \rangle$. The short horizontal line on the right is the high-temperature asymptote $u_\infty(\alpha)$ [Eq. (5.34)], and the longer horizontal line is $u_{\max}$, the upper intercept of the bottom branch at $T = 0$ [Eq. (5.14)].

A. Average displacement and free energy

The last graphs in Sec. IV (Figs. 4 and 5) showed there is no phase transition with an asymmetric on-site potential and $\alpha = 0$. Figure 6 shows the result of increasing the anharmonicity strength; for $\alpha = 0.045$, the top branch of $\langle u \rangle$ vs T has become steeper. The free energy f for this case has the same general shape as in Fig. 5. The branch of f corresponding to the top branch of $\langle u \rangle$ vs T (Fig. 6) always has lower values than the branch of f corresponding to the lower branch of $\langle u \rangle$ vs T, and so it is the equilibrium solution. The equilibrium state of the system, i.e., the state of minimum free energy, follows the arrow in Fig. 6 for increasing T (and the reversed path for decreasing T). There are no discontinuities or singularities and thus still no phase transition for this α value.

For further increases in α, the top branch of $\langle u \rangle$ vs T becomes even steeper. One can visualize from Fig. 6 that at a *critical* value α_c the top branch develops an infinite slope at a certain T. We do not have an analytic method to determine α_c, but numerically we have found $\alpha_c = 0.0576\ldots$. The critical value found in MD was $\alpha_c^{(\mathrm{MD})} \approx 0.124$. (The value obtained in paper II was $\alpha_c = 0.0537\ldots$.) These values of course depend on the values of the other parameters D, a_0, and k.

For larger α values the top branch of the $\langle u \rangle$ vs T graph folds back and becomes multivalued over a certain temperature interval, so that a first-order transition develops. Figure 7 shows the solution for $\alpha = 0.0615$, where the multivalued nature is evident. The corresponding free energy function is shown in Fig. 8. On the temperature interval where the top branch of $\langle u \rangle$ vs T is multivalued, the free energy also develops a loop, similar to the free energy function in the van der Waals theory of the nonideal gas.[8] [The loop occurs near the maximum in Fig. 8(a) and is shown on an expanded scale in Fig. 8(b).] Since the thermal equilibrium state is the one of minimum f, the transition is at the temperature T_c where the free energy graph intersects itself. At this temperature the system undergoes a discontinuous change in $\langle u \rangle$. The entropy is $s = -\partial f / \partial T$, and so it increases discontinuously at the transition, as expected from the argument in the Introduction. The transition temperature is marked by a vertical line on the $\langle u \rangle$ vs T graph (Fig. 7); the line shows the discontinuity in $\langle u \rangle$. For this α value the jump is between two points on the same solution branch of the SCMFT equations. The arrows on the top branch of $\langle u \rangle$ vs T show the sequence of equilibrium states followed by the system. For increasing T, the system evolves out of the stable minimum of the on-site potential, follows the curve until it reaches the vertical line at T_c, and then jumps to the lower part of the same curve. The points on the loops cut off by the vertical line are solutions of the SCMFT equations, but they are inaccessible for thermal equilibrium states. Parts of these loops may be metastable states achievable by superheating or supercooling.

The bottom panel of Fig. 7 shows $\langle u \rangle$ vs T with an expanded vertical scale and a compressed horizontal scale. In contrast to the case in Fig. 6, the approach to the high-T asymptote here is nonmonotonic; $\langle u \rangle$ goes below $u_\infty(\alpha)$

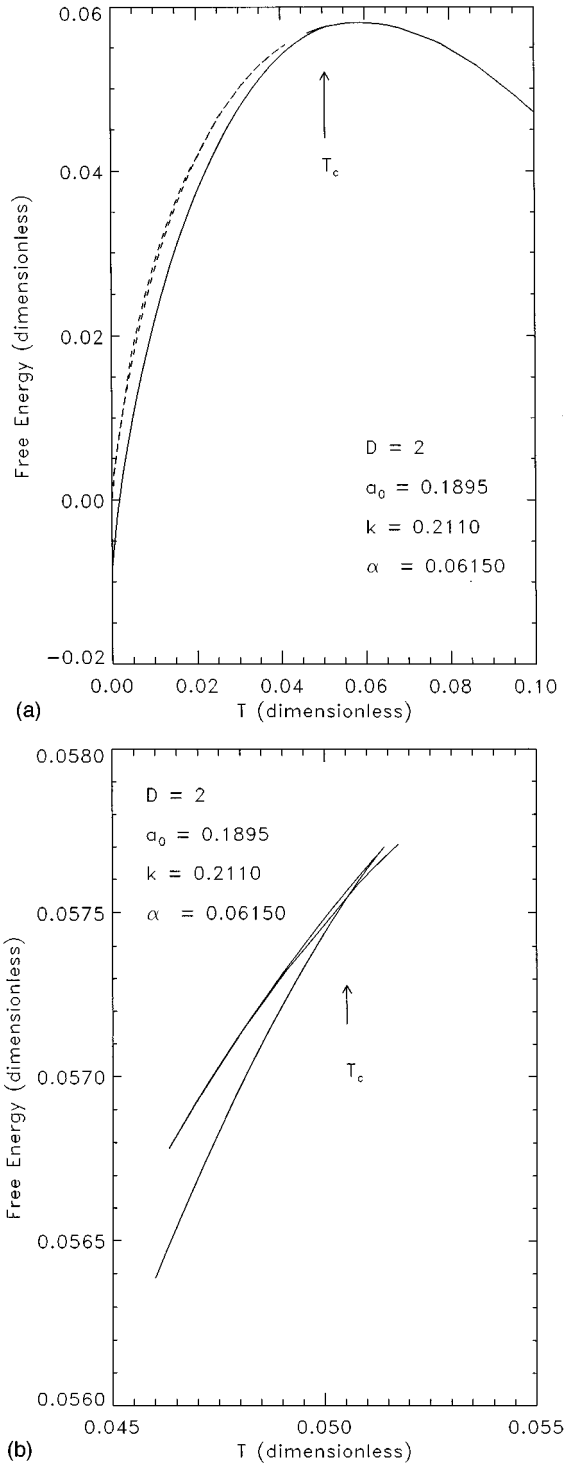

FIG. 8. The free energy corresponding to the solution in Fig. 7. (a) Free energy for both branches of Fig. 7. The solid curve corresponds to the top branch of Fig. 7 and contains the equilibrium solution. The dashed curve is a very narrow loop corresponding to the lower branch of Fig. 7. (b) Expanded view near the maximum of (a), showing the loop in the free energy. T_c, the temperature at which this curve intersects itself, is transferred to Fig. 7.

(marked with the short horizontal line), and then approaches it from below. The longer horizontal line on the bottom panel of Fig. 7 marks $u_{\max}$, the maximum of the on-site potential; it may be considered the dividing point between the stable

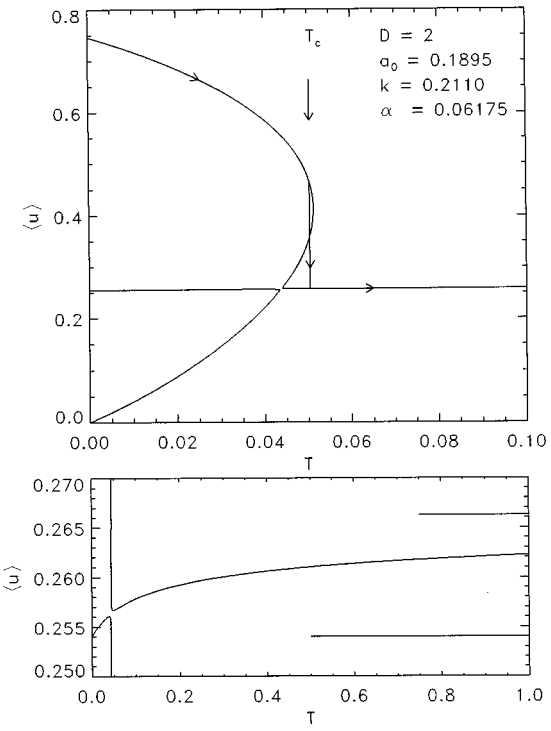

FIG. 9. Average displacement vs temperature for $\alpha = 0.061\,75$, just below the switchover value. The arrows on the top panel and the horizontal lines on the bottom panel are defined as in Fig. 7.

and metastable wells. Since all points on the upper branch of $\langle u\rangle$ vs T are greater than $u_{\max}$, the jump in $\langle u\rangle$ at T_c occurs between a position of low on-site potential energy and a higher-energy position, and both are in the stable well of the on-site potential. This observation is interesting from the point of view of understanding the mechanism which drives the transition. Even though this discontinuity in $\langle u\rangle$ for increasing T results in the particles moving into a region of higher on-site potential energy, this jump in $\langle u\rangle$ is thermodynamically preferred. The reason that the transition is thermodynamically preferred must be that the entropy of the system substantially increases with this jump.

The slope of the $\langle u\rangle$ vs T graph at the three $T = 0$ intercepts is given in Eq. (5.24). For the intercept at $u_{\max}$, $V_1''(u_{\max})$ is negative, and for the value of k used here, $K_{\max}$ [Eq. (5.22)] is positive for all α. For increasing α, this slope changes sign from negative to positive when $u_2(\alpha)$ [Eq. (5.26)] decreases through $u_{\max}$, which occurs at $\alpha = 0.0594\ldots$. This change in slope at $u_{\max}$ is evident in Fig. 6 and the bottom panel of Fig. 7. The details of these slope changes and the interplay of the asymptotic value $u_\infty(\alpha)$ with the extrema of the on-site potential is more intricate in this self-consistent theory than was found in paper II.

For further increases in α, the top branch of $\langle u\rangle$ vs T bends back more sharply, and the high-temperature asymptote $u_\infty(\alpha)$ [Eq. (5.34)] decreases. At another critical value, which we call the *switchover* value, α_s, the two branches of the $\langle u\rangle$ vs T graph come into contact and then reconnect in a different shape. Figures 9–11 show the situation just below and just above this switchover. Just as for α_c, we have not found an analytical evaluation of α_s, but numerically we

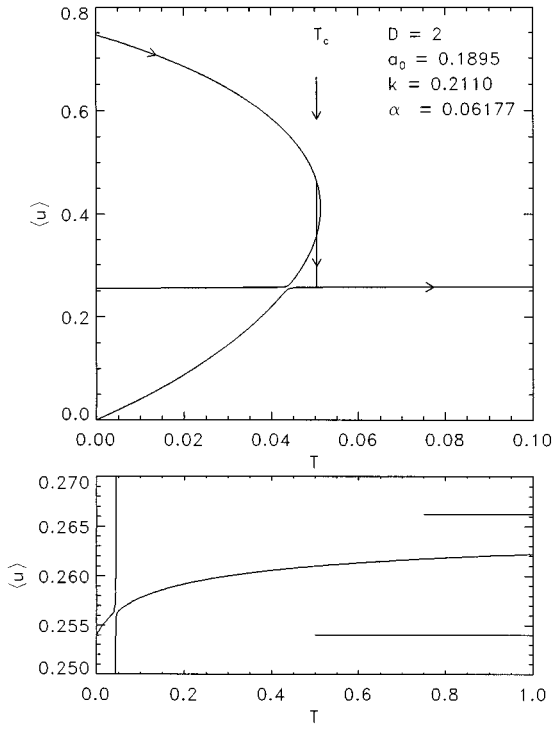

FIG. 10. Average displacement vs temperature for $\alpha = 0.061\,77$, just above the switchover value, showing that pieces of the solution curves have reconnected, and that the jump at the transition is now between different branches of the curves. The arrows and horizontal lines have the same meaning as in Fig. 7, except that $u_{\max}$ is now the lower intercept of the top branch. The points on the top branch which are lower than the highest point on the vertical line showing the jump at T_c are solutions of the SCMFT equations but are not accessible in thermal equilibrium. The same is true of the points on the bottom branch which are to the left of the vertical line.

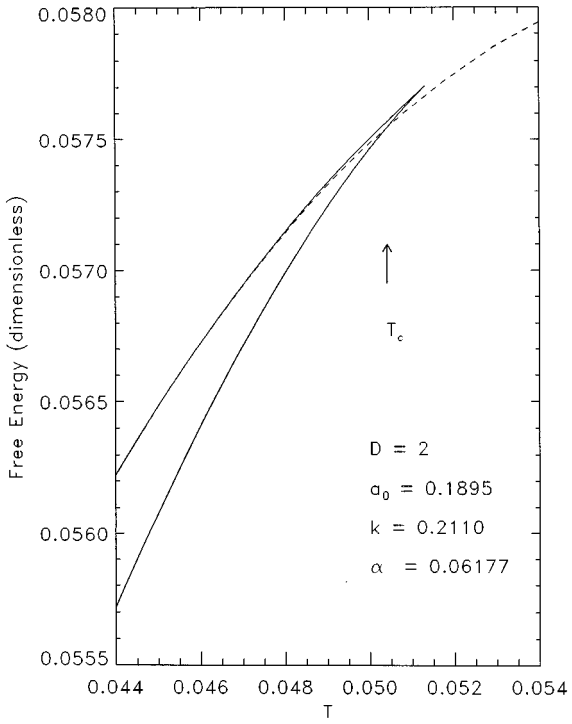

FIG. 11. The expanded piece of the free energy graph corresponding to Fig. 10, showing how the curves for the two branches cross at the transition. The solid curve corresponds to the top branch of Fig. 10, and the dotted curve to the bottom branch. There is no loop in the free energy graph for α above the switchover value.

have found that it lies in the interval $0.061\,76 < \alpha_s < 0.061\,77$ (for the given values of the other parameters). For the average displacement curves, there is actually little change in their ''local'' shapes, but they change ''globally.'' For $\alpha > \alpha_s$, the jump at T_c is between different branches of the solution, but the magnitude of the discontinuity in $\langle u \rangle$ is a continuous function of α through this switchover. The change in the shape of the free energy graph is more pronounced. For $\alpha < \alpha_s$, there is a loop in one branch of the free energy curve, and this loop has upper and lower stability temperatures. For $\alpha > \alpha_s$, there is no longer a loop, and there is only an upper stability temperature. The authors of paper II speculated that the existence of these stability temperatures is related to the hysteresis seen in the computer simulations in paper I. The more complicated self-consistent theory in this paper has the same shapes for the solution curves and so supports the same speculation.

The lower panels of Figs. 9 and 10 show the same nonmonotonic approach to the high-temperature asymptote that was observed in Fig. 7. In Fig. 10 the region of the $\langle u \rangle$ vs T graph near the point where the two branches approach each other is multivalued in both directions, i.e., with either T or $\langle u \rangle$ considered as the independent variable.

The high-temperature asymptote $u_\infty(\alpha)$ [Eq. (5.34)] decreases with increasing α, and so eventually it becomes less than $u_{\max}$; then the jump in $\langle u \rangle$ at T_c is between points in different wells of the on-site potential. Figure 12 shows $\langle u \rangle$ vs T for $\alpha = 0.074$, where this situation has occurred. As in the previous figures, the arrows show the thermal equilibrium states followed for increasing T. The parts of the curves not reached by following the arrows are solutions of the SCMFT equations, but are not accessible in thermal equilibrium.

For a final case, in Fig. 13 we show $\langle u \rangle$ vs T for $\alpha = 0.28$. At this value, the slope of the lower branch of $\langle u \rangle$ vs T coming out of the $\langle u \rangle = 0$ intercept is negative [Eq. (5.24)], while the high-temperature asymptote $u_\infty(\alpha)$ is positive. This means that the jump in $\langle u \rangle$ at T_c is from the stable well of the on-site potential to a point on the negative side of the metastable well. Then $\langle u \rangle$ moves across the metastable well to the positive side as T is increased. Increasing α further eventually decreases $u_\infty(\alpha)$ to negative values, and then $\langle u \rangle$ remains negative for all $T > T_c$.

In Fig. 14 we show the dependence of T_c on α, along with the results of the MD simulations from paper I.[9] These SCMFT results are shifted horizontally relative to the simulation results, i.e., the critical value of α according to the simulations is $\alpha_c \approx 0.124$ (this is the MD point at the smallest α), whereas the SCMFT gives $\alpha_c = 0.0576\ldots$. The simulations were done before the existence of the switchover in the shape of the $\langle u \rangle$ vs T graphs was known, and so there is no comparison available for those values. The decrease in T_c with increasing α is reasonable from the assertion that the

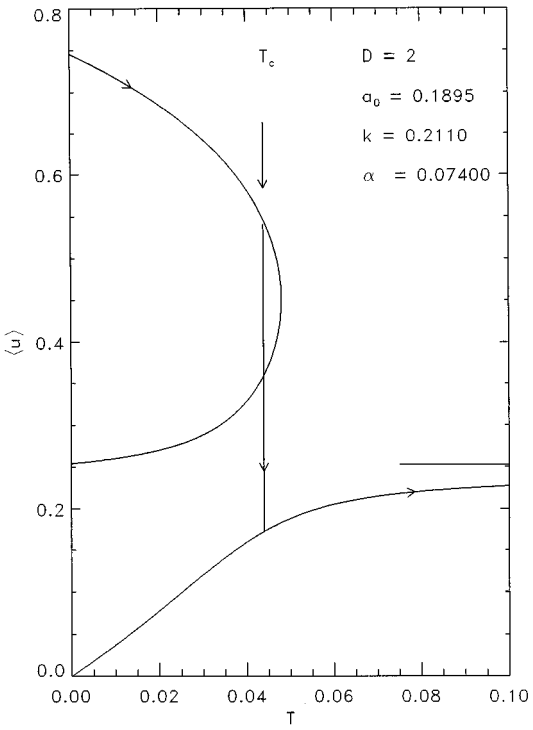

FIG. 12. Average displacement vs temperature for $\alpha = 0.074$, where $u_\infty(\alpha)=0.253\ldots$ is below $u_{\max}=0.254\ldots$.

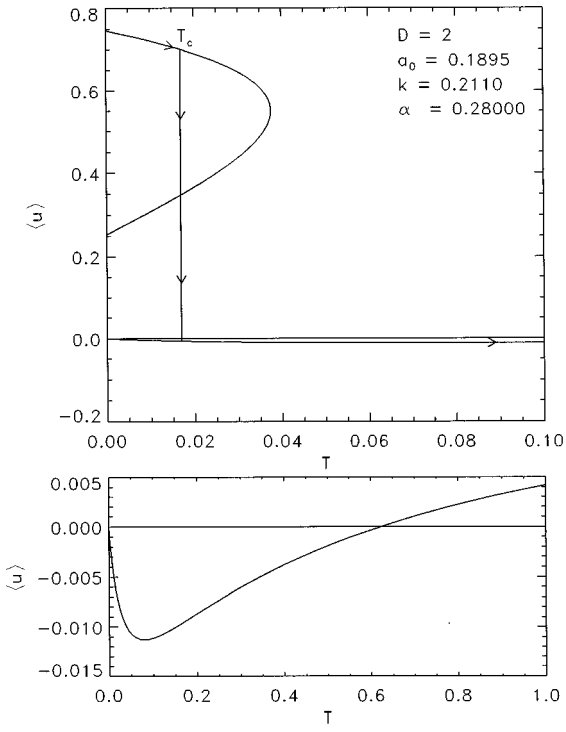

FIG. 13. Average displacement vs temperature for $\alpha = 0.28$. For this α value, the bottom branch starts from zero at $T = 0$ with negative slope [Eq. (5.24)], but $u_\infty(\alpha)=0.0292\ldots$ is positive.

transition is entropy driven; an increase in the anharmonicity strength allows the disordering effect to occur at a lower temperature.

B. Displacement probability distribution functions

From the solutions of the SCMFT equations, we obtain the displacement PDF $P_1(u)$ from Eq. (3.10). We show this function for $\alpha = 0.074$ in Fig. 15. The results for all of the other α values considered in this section have the same general features. The arrows on the graph locate the three extrema of the on-site potential [Eq. (2.3)]. The graphs show that the PDF is localized in the stable well at low T. The second and third T values are just below and just above T_c, and so the distribution jumps, corresponding to the discontinuity in $\langle u\rangle$ shown in Fig. 12. (The magnitude of this jump increases with increasing α, as can be inferred from the magnitude of the discontinuity in $\langle u\rangle$ shown in Figs. 7, 9, 10, 12, and 13.) Since $\alpha>\alpha_s$ in Fig. 15, for high T values the distribution shifts towards positive values, corresponding to the increase in $\langle u\rangle$ for $T>T_c$ shown in Fig. 12. The bottom curve in Fig. 15, at a considerably higher T, shows that the maximum in the curve, which is the quantity $u_p(T)$ discussed at length in Sec. V, continues to increase while the average value $\langle u\rangle$ remains finite [see Eqs. (5.33) and (5.34)].

The shapes of these PDFs can be characterized by two of their moments: the skewness

$$S[P_1]=\int_{-\infty}^{\infty} du\left(\frac{u-\langle u\rangle}{\sigma}\right)^3 P_1(u) \tag{6.1}$$

and the kurtosis

$$K[P_1]=\int_{-\infty}^{\infty} du\left(\frac{u-\langle u\rangle}{\sigma}\right)^4 P_1(u)-3. \tag{6.2}$$

Here σ is the standard deviation of the distribution. The skewness measures the asymmetry of the distribution, and the kurtosis measures its peakedness or flatness.[10] Positive skewness indicates an asymmetric tail extending toward positive u (and the reverse for negative skewness). Similarly, positive kurtosis denotes a more peaked distribution, whereas negative kurtosis denotes a flatter distribution (relative to a Gaussian, which has zero kurtosis).

The skewness and kurtosis for $\alpha = 0.074$ are shown as functions of T in Fig. 16. The skewness shows that the distributions have substantially more weight towards smaller displacements below T_c; this feature indicates the tendency of the particles to move away from the strongly repulsive part of the on-site potential toward the less repulsive region. Above T_c the distributions have a somewhat more weight towards smaller displacements, but not to the degree as below T_c. The kurtosis indicates that the distributions are more peaked below T_c and flatter above T_c.

From this PDF we can analyze the possibility of transformation precursors, i.e., clusters of particles displaced into the structure which is ''wrong'' compared to the equilibrium structure at the ambient temperature. Clusters which are sufficiently large or numerous would produce multipeaked PDF's. However, only single-peaked PDF's were found for the parameter values and temperatures used in these calculations. But that does not mean there are no particles displaced into such regions, and in fact Fig. 15 shows the PDF's extending into both wells of the on-site potential for all but the lowest T values. One characterization of this possibility is to

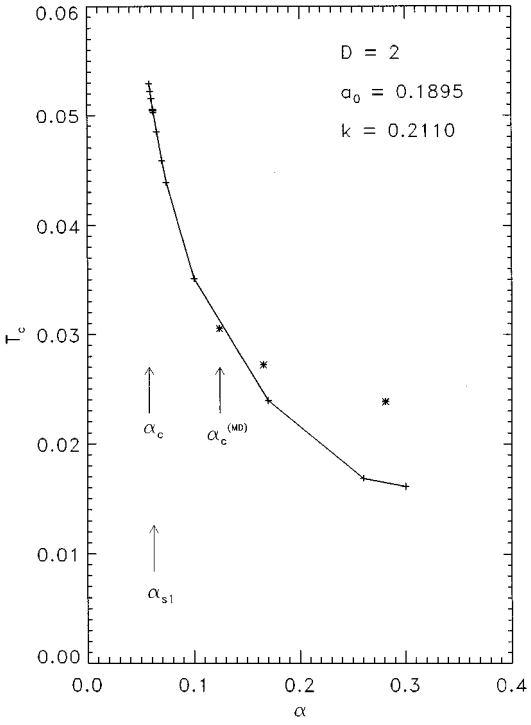

FIG. 14. Dependence of the transition temperature on the anharmonicity parameter α. The SCMFT values for the minimum value to have a transition α_c and the switchover value α_s are marked. The approximate value of α_c determined from the MD is also marked. The three isolated points shown are the results from the MD calculations in paper I.

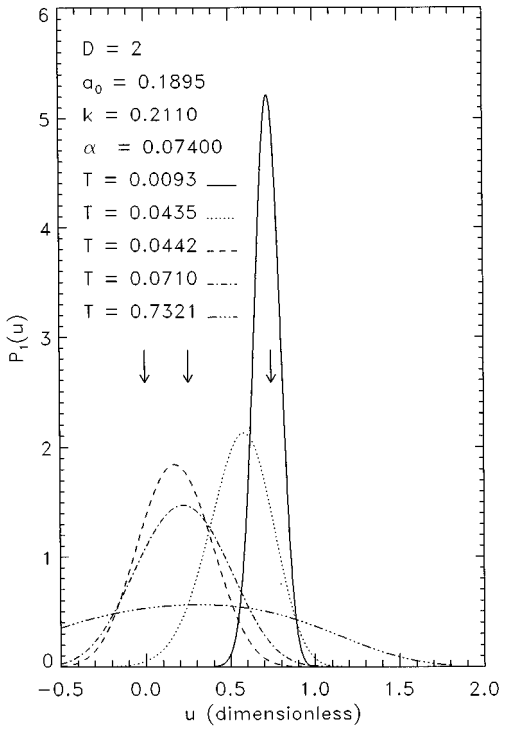

FIG. 15. Displacement probability distributions for $\alpha = 0.074$, for different temperatures. The second and third T values are just below and just above $T_c = 0.0439\ldots$ for this α value. The vertical arrows denote the three extrema of the on-site potential [Eq. (2.3).]

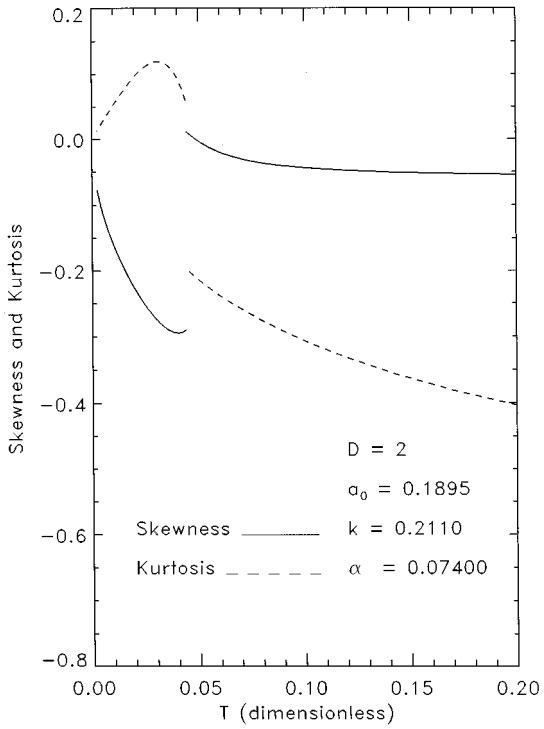

FIG. 16. Skewness and kurtosis of the displacement probability distributions for $\alpha = 0.074$. The discontinuity occurs at T_c.

consider the fraction of particles in one of the wells, e.g., the metastable well. That fraction is

$$P(u<u_{\max}) = \int_{-\infty}^{u_{\max}} du P_1(u), \tag{6.3}$$

and is a function of α and T. This number is given in Table I for different α values and for two temperatures just below and just above the T_c value for that α. For T just below T_c and for the range $\alpha_c<\alpha<\alpha_s$, the fraction of particles in the metastable well is around 0.15. For T just above T_c, the fraction in the metastable well (the ''correct'' phase for this T) increases to a value around 0.5 or more. However, we found no situation where these fluctuations are large enough to produce a second maximum in $P_1(u)$.

For $\alpha>\alpha_s$ the fraction of particles in the ''wrong'' phase (both below and above T_c) decreases rapidly. This indicates that the PDF's narrow quite rapidly for increasing anharmonicity strength. Partly this is because the transition temperature T_c decreases with increasing α. However, the widths of $P_1(u)$ decrease more rapidly than T_c does (see Fig. 14),

TABLE I. $P(u<u_{\max})$, the probability that the displacements are in the metastable well, for different α values and for temperatures just below and just above $T_c(\alpha)$. (E.g., the row for $\alpha = 0.074$ corresponds to the two curves in Fig. 15 at $T = 0.0435$ and 0.0442.)

α	$T<T_c$	$T>T_c$
0.0615	0.155	0.489
0.06175	0.155	0.494
0.074	0.0669	0.648
0.28	7.21×10^{-7}	0.985

indicating that increasing the anharmonicity strength tends to localize the particles into the ''correct'' well. The PDF's obtained in the simulation exhibit this same narrowing with increasing α; see Figs. 14 and 15 of paper I.

Another characterization of the lack of transformation precursors is obtained by applying to this system the criterion used by Gooding and Morris.[11] Their method, applied to this model, is to follow the value of $P_1(u_{\min})$ as T approaches T_c from above, i.e., to follow the T dependence of the probability for a particle to be displaced into the low-temperature structure when the system is in the high-temperature phase and approaching the transition. Figure 15 shows that $P_1(u_{\min})$ *decreases* for $T \rightarrow T_c+$. The probability concentrates more into the metastable well, and fluctuations into the low-temperature structure decrease as T decreases to T_c. Gooding and Morris reached the same conclusion based on their model and method of analysis. However, we note that for our model this conclusion applies only to cooling. Figure 15 shows that the probability of displacement to the metastable minimum $P_1(u_{\rm ms})$ increases for T approaching T_c from below.

In Sec. V A we argued that the system properties would be different with a weaker force constant k. This change would increase the importance of the on-site potential relative to the interparticle interactions, and so multipeaked PDF's seem to be more likely in this regime. Since the parameters were chosen to represent the experimentally relevant case of Zr (see Sec. II), we have not analyzed this other possibility in this paper.

VII. SUMMARY

In this paper we have presented a self-consistent mean-field theory for a lattice-dynamical model that exhibits a first-order structural phase transition. The essential features of the model are (i) each particle moves in an asymmetric double-well on-site potential and (ii) anharmonicity is included in the interparticle interactions. The second feature is crucial: Without this anharmonicity there is no phase transition. This anharmonicity provides a mechanism that increases the entropy of the high-energy structure relative to the low-energy structure and thereby achieves a lower free energy at sufficiently high temperatures.

We obtained the mean field in the following way. In the exact equation of motion for a particular particle, all occurrences of any quantity associated with a neighboring particle are replaced by the average value of that quantity. This replacement is equivalent to assuming that the phase space PDF factors into a product of single-particle PDF's. It gives rise to an effective potential governing (approximately) the motion of any one particle. The averages are then obtained self-consistently through the Gibbs distribution determined by the effective potential. The resulting solutions are used to survey thermodynamic properties in a portion of the parameter space. The regions of parameter space studied here covered a wide range of strength for the interparticle anharmonicity but for only a single value for the harmonic force constant. This value is in the so-called displacive regime where local quantities change slowly with respect to lattice site.

We summarize the results of this theory and compare them with the simulations in paper I. All of the qualitative features of the theory also appear in the simulations. The results are the following. (1) A critical strength α_c of the interparticle anharmonicity is needed for a phase transition to occur. This feature agrees with the simulations, but the MFT and the simulations disagree about the value of α_c. (2) According to this MFT there are two intervals of interparticle anharmonicity strength above the critical value, within which the thermodynamic properties are different. For the interval of weaker strength, the free energy has a van der Waals–type loop in it. For the interval of greater strength (which is a much larger interval) there is no such loop. The free energy was not calculated in the simulations, but they exhibited a feature which we speculate is related to this change in the shape of the MFT free energy function. The simulations were mostly performed for a large value of α, and they exhibited hysteresis. The hysteresis loops were ''open,'' in the sense that a transition was obtained only for heating and not for cooling (see Fig. 3 of paper I). We speculate that this feature is related to the presence or absence of a loop in the free energy. The existence of a loop, as in Fig. 8(b), implies the existence of upper and lower stability limits for temperature. If the system is heated or cooled into the metastable region beyond T_c, it cannot be heated or cooled beyond the end points of the loop without changing phase. Conversely, if there is no loop, as in Fig. 11, then there is a stability limit for heating the system from low temperature, but there is no stability limit for cooling it from high temperature. This second situation is the one that obtained in the simulations. We are presently performing simulations at smaller α values to see if closed hysteresis loops are obtained.[12] (3) This theory and the simulations agree that the displacement PDF's are nearly symmetric and have only one maximum for the parameter values used by both methods. The MFT indicates that this feature persists over a wider range of anharmonicity strength than was studied by the simulations. The possibility to have multiple maxima is equivalent to having multiple minima in the effective potential. Since this function is a quartic polynomial with temperature-dependent coefficients, having several extrema is possible, but we did not find such a situation for the parameters studied here. However, we argued that such PDF's might be found for weaker interparticle forces where the effect of the on-site potential would be relatively larger. (4) This MFT predicts that for quite large temperature, the displacement PDF becomes asymmetric in a particular way: The mean value of the distribution remains finite whereas the most likely value moves out to infinity. This feature depends only on the interparticle anharmonicity controlled by the parameter α. The simulations in paper I did not go to high enough T to see this effect.

Next we compare the results of the present theory with the results in paper II, which also presented a MFT of this model. That earlier MFT made an additional assumption that the displacement PDF is Gaussian. The results of the present theory show how accurate that assumption is (see Figs. 15 and 16), for the parameter values used in both papers. The quantitative results of this theory are similar to those in paper II; e.g., there are only small shifts in the ''critical'' and ''switchover'' values of α. The value of α_c in the present theory is somewhat closer to the simulation value. There are two major qualitative differences between these two mean-

field theories. The first, discussed in the paragraph above, is that the present theory allows the possibility of double-peaked PDF's. The second is that the shapes of the $\langle u \rangle$ vs T relation are more intricate in the present theory. The nonmonotonic approach to the high-temperature asymptote seen in Fig. 9, the overlapping of the two branches of the relation seen in the bottom panel of Fig. 10, and the change in sign of $\langle u \rangle$ vs T seen in Fig. 13 are features that could not be obtained with the method in paper II.

To conclude, we suggest a possible experimental measurement based on the observation about the different behavior of $\langle u \rangle$ and $u_p(T)$ at high temperature [item (4) above]. The Fourier transform of the displacement PDF is $\langle \exp(iku) \rangle$, which is the Debye-Waller factor measured by x-ray diffraction or Mössbauer spectroscopy. In principle, the displacement PDF can be measured by these techniques. If an experiment on a structurally transforming system obtained a PDF with asymmetry as described above, that result would be evidence that the mechanism driving the transition is the one utilized in this model.

ACKNOWLEDGMENTS

This work was supported in part by NSF Grant No. DMR-9403009 to Wake Forest University. W.C.K. thanks the Condensed Matter and Statistical Physics Group of the Theoretical Division at Los Alamos National Laboratory for their hospitality during a sabbatical leave. The Laboratory is supported by the U.S. DOE.

APPENDIX

We mention briefly the numerical techniques we used to solve the SCMFT equations, Eqs. (3.7) and (3.8). To evaluate the integrals, we used the formula for the reduced moments obtained for the low-temperature expansion in Eq. (5.7). This form is suitable for numerical evaluation by the Gauss-Hermite method. Similarly, the form used for the high-temperature expansion in Eq. (5.28) is suitable for numerical evaluation by the Gauss-Laguerre method. We mostly used the former method, except for those parts of the $\langle u \rangle$ vs T graphs that extend out to the highest temperatures.

For the Gauss-Hermite method we found that we could achieve convergence of the integrals to higher temperatures if we did *not* shift the origin of the integration variable to the peak of the probability distribution, as we did for the asymptotic expansions in Sec. V [see Eq. (5.3)]. Instead we found that a smaller shift works better. Such a shift leaves a linear term in the exponent, but the Gauss-Hermite method is still applicable.

We solved the SCMFT equations by Newton's method. For very low or very high temperatures, the initial guesses were obtained from the asymptotic expansions in Sec. V. For subsequent increments of the independent variable, the result from the previous step was used as the guess for the new step. Because of the nonmonotonicity of the $\langle u \rangle$ vs T curves, (e.g., the bottom panel of Fig. 7) we found it useful to have two procedures; one took $\langle u \rangle$ as the independent variable and solved for T, and the other reversed those variables. Then the outputs were merged to produce the graphs.

---

*Permanent address.

[1] W. C. Kerr, A. M. Hawthorne, R. J. Gooding, A. R. Bishop, and J. A. Krumhansl, Phys. Rev. B **45**, 7036 (1992). This paper will be referred to as paper I.

[2] W. C. Kerr and M. J. Rave, Phys. Rev. B **48**, 16 234 (1993). This paper will be referred to as paper II.

[3] C. Zener, Phys. Rev. **71**, 846 (1947).

[4] A. D. Bruce, Adv. Phys **9**, 111 (1980).

[5] J. R. Morris and R. J. Gooding, Phys. Rev. Lett. **65**, 1769 (1990); R. J. Gooding, Scr. Metall. **25**, 105 (1991); J. R. Morris and R. J. Gooding, Phys. Rev. B **43**, 6057 (1991); **46**, 8733 (1992); J. Stat. Phys. **67**, 471 (1992); R. J. Gooding and J. R. Morris, Phys. Rev. E **47**, 2934 (1993).

[6] G. Parisi, *Statistical Field Theory* (Addison-Wesley, Redwood City, CA, 1988), p. 24.

[7] See Sec. 3 of Ref. 4, where a detailed comparison of the two methods for the ϕ^4 model is given.

[8] See, e.g., C. Kittel and H. Kroemer, *Thermal Physics* (Freeman, San Francisco, 1980), p. 293.

[9] The MD results from paper I show the transition temperature found when *heating* the system. The simulations exhibited considerable hysteresis for heating and cooling, and so these MD values are undoubtedly higher than the equilibrium T_c.

[10] See, e.g., W. H. Press, S. A. Teukolsky, W. T. Vetterling, and Brian P. Flannery, *Numerical Recipes in C* (Cambridge University Press, New York, 1992), p. 612.

[11] See the last paper listed in Ref. 5.

[12] W. C. Kerr (unpublished).